Influence of cathode opening size and wetting properties of diffusion layers on the performance of air-breathing PEMFCs

A. Schmitz *, M. Tranitz, S. Eccarius, A. Weil, C. Hebling

Fraunhofer Institute for Solar Energy Systems, Heidenhofstr. 2, D-79110 Freiburg, Germany

Available online 9 December 2005

Abstract

Air-breathing PEMFCs consist of an open cathodic side to allow an entirely passive supply of oxygen by diffusion. Furthermore, a large fraction of the produced water is removed by evaporation from the open cathode. Gas diffusion layers (GDLs) and the opening size of the cathode have a crucial influence on the performance of an air-breathing PEMFC. In order to assure an unobstructed supply of oxygen the water has to be removed efficiently and condensation in the GDL has to be avoided. On the other hand good humidification of the membrane has to be achieved to obtain high protonic conductivity.

In this paper the influence of varying cathodic opening sizes (33%, 50% and 80% opening ratios) and of GDLs with different wetting properties are analysed. GDLs with hydrophobic and hydrophilic properties are prepared by coating of untreated GDLs (Toray® carbon paper TGP-H-120, thickness of 350 μm). The air-breathing PEMFC test samples are realised using printed circuit board (PCB) technology.

The cell samples were characterised over the entire potential range (0–0.95 V) by extensive measurements of the current density, the temperature and the cell impedance at 1 kHz. Additionally, measurements of the water balance were carried out at distinct operation points.

The best cell performance was achieved with the largest opening ratio (80%) and an untreated GDL. At the maximum power point, this cell sample achieved a power density of $100 \, \text{mW cm}^{-2}$ at a moderate cell temperature of 43 °C. Furthermore, it could be shown that GDLs with hydrophilic or intense hydrophobic properties do not improve the performance of an air-breathing PEMFC.

Based on the extensive characterisations, two design rules for air-breathing PEMFCs could be formulated.

Firstly, it is crucial to maximise the cathode opening as far as an appropriate compression pressure of the cell assembly and therewith low contact resistance can be assured. Secondly, it is advantageous to use an untreated, slightly hydrophobic GDL.
© 2005 Elsevier B.V. All rights reserved.

Keywords: Air-breathing PEMFC; Water management; Planar PEMFC; Hyrophobic and hydrophilic diffusion layer; Geometry variation; Printed circuit board (PCB)

1. Planar air-breathing design of PEMFC

Miniaturized fuel cells offer new opportunities as a possible replacement of battery systems. The recent development of miniaturized fuel cells is driven by the increasing power and energy need of electronic devices [1,2]. The PEMFC is a promising alternative to batteries as power supply in consumer electronics, sensors, and medical devices.

For a successful integration of fuel cells into electrical appliances, the dimension of the fuel cell must be in accordance with the existing geometry of the device. In most devices it is required that the geometry of the power supply is rather flat in order to obtain a compact and practical design. This means that it can be difficult to integrate a fuel cell with a conventional stack design into such a device.

In order to achieve higher output voltages, a plurality of single fuel cells has to be series-connected. In the conventional design the fuel cells are stacked one upon the other (stack design) and the electrical connection is realised by bipolar plates, which separate anodic and cathodic compartment of the adjacent cells. However, the stack design is not suited to construct flat fuel cell systems.

In a planar series-connected PEMFC, the single cells are located adjacent to each other in such a way that the MEA-areas of each cell are located in one plain. Thus, all anodes of the cell are on the one side of this plain and all cathodes are on the other side. The series connection in the planar design is realised by electrical connection of an anode, with the cathode of the adjacent cell, through this plain.

* Corresponding author.
  E-mail addresses: astz@gmx.net, schmitza@imec.be (A. Schmitz).

Series-connected planar PEMFCs have recently been demonstrated in printed circuit board technology (PCB) [3–5]. PCB plates consist of a fibre glass epoxy composite material. Due to their composition, PCB plates are very rigid and lightweight. Using PCB technology, series-connected planar PEMFCs in a very thin (<3 mm) and lightweight design have been realised. Long-term stability of this type of fuel cell for more than 1500 h has been demonstrated [6,7]. Furthermore, PCB technology is a well-known and flexible mass production process. This capability allows to manufacture different designs of planar fuel cells at low cost.

Passive air-breathing operation of planar PEMFCs can be achieved by using a cathode, which is open to the exterior. In this design, oxygen is supplied in an entirely passive manner by diffusion. Similarly, the water produced in the fuel cell reaction is removed by evaporation from the open cathode.

An important advantage of the passive air-breathing operation is that an active supply of air, by pumps or fans is not needed. Thus, parasitic power losses by auxiliary components can be avoided.

Due to the passive air-breathing operation, the opening size of the cathode and the porous structure of the gas diffusion layers are crucial to improve the supply of oxygen. Moreover, water management is an important issue for air-breathing operation. In order to assure an unobstructed supply of oxygen the water has to be removed efficiently and condensation in the gas diffusion layer (GDL) has to be avoided. On the other hand good humidification of the membrane has to be achieved to obtain high protonic conductivity. Thus, the interaction of opening size and properties of the diffusion layers is crucial to optimize the performance of an air-breathing PEMFC. In this paper, an air-breathing PEMFC with different opening sizes of the cathode and different wetting properties are characterised.

2. Construction of air-breathing cell sample

The type of air-breathing PEMFC used in this paper is made of printed circuit boards (PCB). A standard printed circuit board consists of an epoxy fibre glass composite material (thickness 1.5 mm) and a thin copper layer (usually thickness: 35 μm). Due to the epoxy fibre glass composite material the boards are very rigid. The anodic and cathodic plates of the air-breathing PEMFC consist of PCB boards. In the anodic plate, a serpentine flow-field, consisting of a single channel with a depth of 0.8 mm, is machined. The channel and the ribs of the flow-field have a width of 1 mm. The hydrogen supply is realised by tubes, which are attached to the inlet and outlet openings on the backside of the anodic PCB plate. The cathodic plate consists of parallel, rectangular openings. The electrochemical active area of this geometry has a size of 20 mm × 50 mm. In the active area, the copper layer of the PCB, acts as current collector. Outside the active area, the copper layer is used as a current conductor towards the external electrical contacts on the side of the plate. The various components and the assembled cell can be seen in Fig. 1.
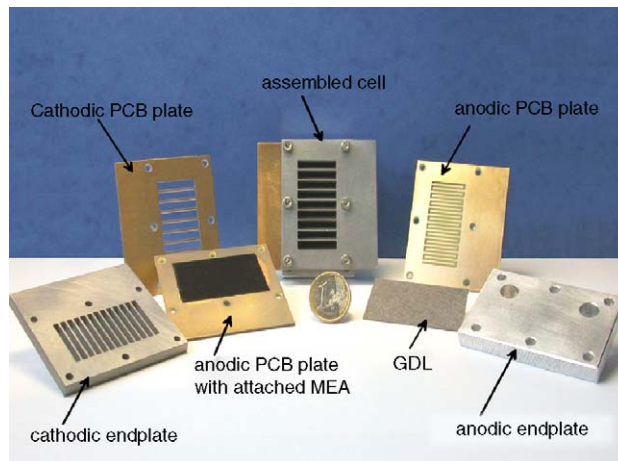

Fig. 1. Depiction of an assembled fuel cell in PCB design and components.

In an assembled cell the GDLs are located between the plates and the MEA. The MEA is attached by adhesives to the anodic plate in order to assure a sealing of the anodic compartment. Additionally, a thin foil with a rectangular opening in the size of the active area is sandwiched between the plates to avoid short circuits between the copper layers. This assembly is pressed together by the use of a cathodic and anodic endplate. The cathodic endplate (steel, thickness: 5 mm) consists of the same openings as the cathode's PCB plate to allow air-breathing operation. The anodic endplate is made of a 15 mm thick aluminium plate. The endplates apply a constant and homogenous contact pressure to the cell assembly, which is crucial to achieve reproducible experimental conditions. Pressure is applied to the endplates by the use of six screws on the edges. By adjusting the torque of these screws, the contact pressure of the whole assembly is controlled.

For the experiments throughout this paper a PRIMEA® 5510 from Gore Associates has been used as a MEA with a Pt loading of 0.3 mg cm^{-2} and an ionomer thickness of 35 μm.

According to the above-described construction sample cells with three different openings were assembled. The geometries of the different cathodic plates are depicted in Fig. 2. The open area ratios of the cathodic plates are 33%, 66% and 80%, respectively. Cell geometry I (opening ratio: 33%) consists of an opening area of 1.5 mm × 20 mm and a rib covered area of 3.0 mm × 20 mm; for cell geometry II (opening ratio: 50%) the open and covered areas are equal (1.0 mm × 20 mm); cell geometry III (opening ratio: 80%) consists of an open area of 4.0 mm × 20 mm and a rib covered area of 1.0 mm × 20 mm. These cells were used as test objects in the experiments presented in the following section.

3. Experimental set-up

A schematic diagram of the measurement set-up used for carrying out the experiments presented in this paper is shown in Fig. 3. In order to characterise the fuel cell at different operation points of its IV-characteristics, a variable electrical load is
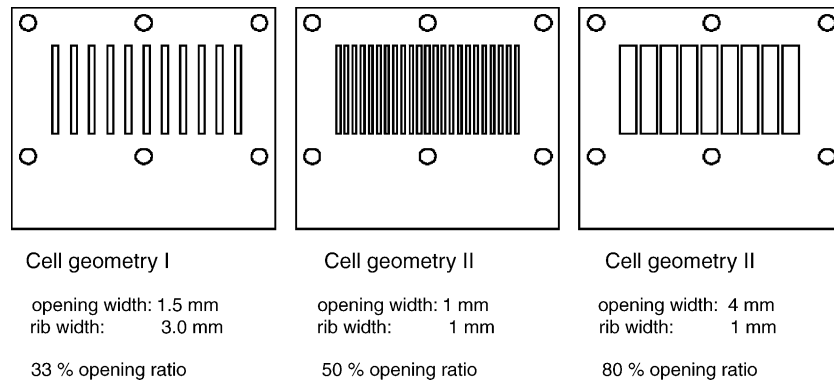
Fig. 2. Depiction of the cathodic plates for the three opening ratios (cell geometries I–III). The electroactive area of the cell has a width of 20 mm and a length of 50 mm.

needed. A Wenking HP88 was used as variable electrical load, which could be operated in galvanostatic or potentiostatic manner.

Moreover, an appropriate and controllable supply of gas must be provided. As the fuel cells examined in this paper are air-breathing, only a supply of hydrogen gas is needed. Flow rates of hydrogen were controlled by means of flowmeters from MKS Instruments (MKS 1179 and PR 4000). Using the flowmeters, a gas flow could be adjusted between 10 and 500 cm^3 min^{-1}. During cell operation the cell temperature was measured using a Pt100. Additionally, the cell impedance at a frequency of 1 kHz could be measured (HP Milliohmmeter 4338B). The high-frequency cell impedance represents the sum of the ionic and electrical resistances. As the ionic resistance of the polymer electrolyte is strongly dependent on the membrane water content, the cell impedance provides information about the humidification of the membrane. Moreover, the amount of water at the anodic side can be assessed. This assessment is realised by condensation of the water in the hydrogen at the cell's outlet using a cryostat. Using this method the water balance can be measured.

4. Influence of opening sizes

As a result of the exothermic electrochemical reaction, heat is produced in the fuel cell. Due to irreversible losses, the amount of heat in the cell increases with decreasing cell potentials [8]. Thus, the cell temperature is highly dependent on the operating point. The temperature influences strongly the kinetics [9] and the mass transport processes [10].

With increasing temperature, more water can be evaporated due to the exponential dependency of the saturation pressure of water on temperature [11]. An augmented evaporation might result in a drying out of the membrane and consequently in an increasing protonic resistance of the membrane.

Since, all these interactions take place at the same time, a real cell has to be considered as a dynamic system. As a consequence, the cell needs some time to reach a steady operation point. In order to observe the stability of cell performance, the cell potential and the current are measured over a certain period of time. For the characterisation of the cell samples, a constant cell potential was applied for about 1 h and the behaviour of the cell current was recorded. This was done in potential steps by
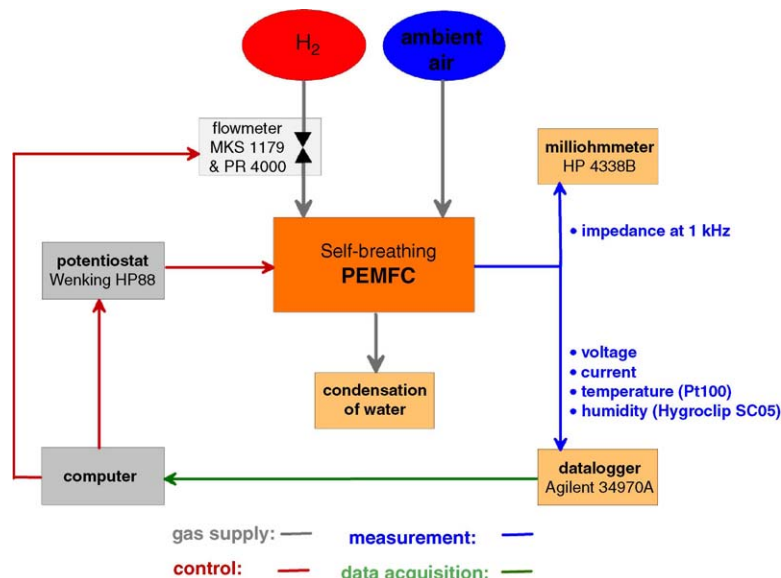

Fig. 3. Schematic diagram of measurement set-up.

starting at 900 mV and decreasing the potential in each step by 100 mV. Using this potential step method, the behaviour of the cell can be observed over a sufficiently long period of time and conclusions on the stability of the cell at certain operating points can be drawn.

Cells samples with the three opening variations mentioned above (Fig. 2) were characterised under ambient and floating temperature conditions. The GDL used on the anodic and cathodic side was Toray® carbon paper TGP-H-120 with a thickness of 350 μm. This carbon paper is wet-proofed. In the original state it shows slightly hydrophobic properties. During the operation, the cells were supplied with dry hydrogen at a flow rate of 55 cm^3 min^{-1}. The characterisation was carried out by measuring the cell current, the cell temperature and the cell impedance at 1 kHz.

For the three opening ratios, the development of the cell current obtained by the potential step method is depicted in Fig. 4a. The dashed curve represents the development of the cell potential. Each potential was applied for a period of 1 h. The cell characterisation starts at a potential of 0.9 V. After 1 h of operating at potentiostatic condition, the cell potential is decreased by 0.1 V. The reaction of the current during the potentiostatic operation is shown in Fig. 4a for the three cathodic opening ratios. By switching to the next potential step, usually higher currents are recorded. Seen at first glance, the reaction of the current is quite stable in most potential steps. The current densities of all cells increase from open circuit conditions to short circuit conditions. In particular, for high currents the behaviour gets more unstable as more water is produced. This can block the GDL. However, at high temperatures the evaporation of water is significantly faster. This can lead to a drying out of the cell, which in turn leads to increased cell impedances causing smaller current densities than potentially achievable. Distinct differences between the cell performance of the three opening ratios are seen. Larger opening ratios result in higher current densities at the same potentials. At short-circuit conditions the current density is 0.155 A cm^{-2} for the cell with the 33% opening ratio, 0.31 A cm^{-2} for the cell with the 50% opening ratio and 0.4 A cm^{-2} for the cell with the 80% opening ratio.

Polarisation curves are extracted from the potential-step characterisations by taking the values of current density and cell potential at the very end of each step. The polarisation curves for the respective openings are depicted in Fig. 4b. Close to open circuit voltage the polarisation curves are almost identical. Significant differences in the shape of the curves can be seen at a higher current density. Mass transport limitations indicated by a rapid decline of the polarisation curve occur in all cases but set on at different cell potentials. The decline of the polarisation curve starts for the smallest opening ratio of 33% at about 0.5 V and for the cell with an opening ratio of 50% at about 0.2 V A cm^{-2}. Mass transport limitations for the cell with the largest opening ratio of 80% occur at a potential as low as 0.1 V and a relatively high current density of about 0.42 A cm^{-2}.

The power characteristics for the three opening ratios are shown in Fig. 4c. At the maximum power point the cell with the 80% opening ratio reaches a power density of 100 W cm^{-2} at a

cell potential of 0.4 V. The maximum power densities achieved with the smaller opening ratios are lower. The cell with the 50% opening ratio reaches a power density of 77 mW cm^{-2} at a cell potential of 0.4 V and the cell with the 33% opening ratio reaches at a power density of 50 mW cm^{-2} at a cell potential of 0.5 V. Hence, the power density for the cell with the largest opening ratio is three times larger compared to the cell with the smallest opening ratio.

Due to the open cathode design, the size of the openings strongly affects the performance of the fuel cell. Larger openings result in an improved supply of oxygen and consequently increasing current densities. Thus, the geometry of the openings and the ribs is a critical issue for the optimised design of planar air-breathing fuel cells.

In addition to the current, the temperature of the cell was measured. During the temperature measurements the Pt100 was placed at the middle of the cathodic opening with thermal contact to the diffusion layer. The development of the cell temperature for the cell samples with different opening ratios is shown in Fig. 4d. With declining cell potentials the temperature decreases from room temperature to a maximum temperature at short circuit conditions. Distinct differences in the development of the cell temperature are seen for the different opening ratios. A temperature of 63 °C is reached for the cell with the 80% opening ratio at short-circuit conditions. The cells with the 33% and 50% opening reach at short-circuit condition a temperature of 51.0 and 40.5 °C, respectively.

Moderate cell temperatures of about 43 °C have been found at the maximum power point of the cell with the 80% opening ratio (100 mW cm^{-2} at 0.4 V). Thus, air-breathing PEMFCs operated at the maximum achievable power density reach a temperature, which corresponds to a temperature slightly higher than the human body temperature.

The cell characterisations are accomplished by the measurement of the cell impedance at 1 kHz (see Fig. 4d). The measurement of the impedance was carried out at the very end of each potential step.

The behaviour of the cell impedance mainly depends on the humidification of the membrane since the protonic conductivity of the membrane is strongly dependent on the water content [12].

In Fig. 4e, the cell impedance as a function of the cell potential is shown for the three opening variations. For cell potentials from 0.9 V to about 0.5 V decreasing cell impedances are seen. This behaviour reflects the self-humidification that results from the increase in water production with decreasing cell potential. In particular, for the cell with the lowest opening ratio (33%, cell geometry I) at cell potentials of 0.9 and 0.8 V significantly higher impedance values are seen when compared to the cells with the larger opening ratios. This phenomenon can be explained by the following facts. First, the exchange with the humid, ambient air is hindered by the broad ribs (3 mm width) of the cell with the lowest opening ratio. Second, the cells were operated with dry hydrogen. Finally, the water production at high cell potentials is very low. For the cell with the lowest opening ratio, the combination of these facts results in a much dryer membrane and consequently higher impedances compared to the cells with the other opening ratios.
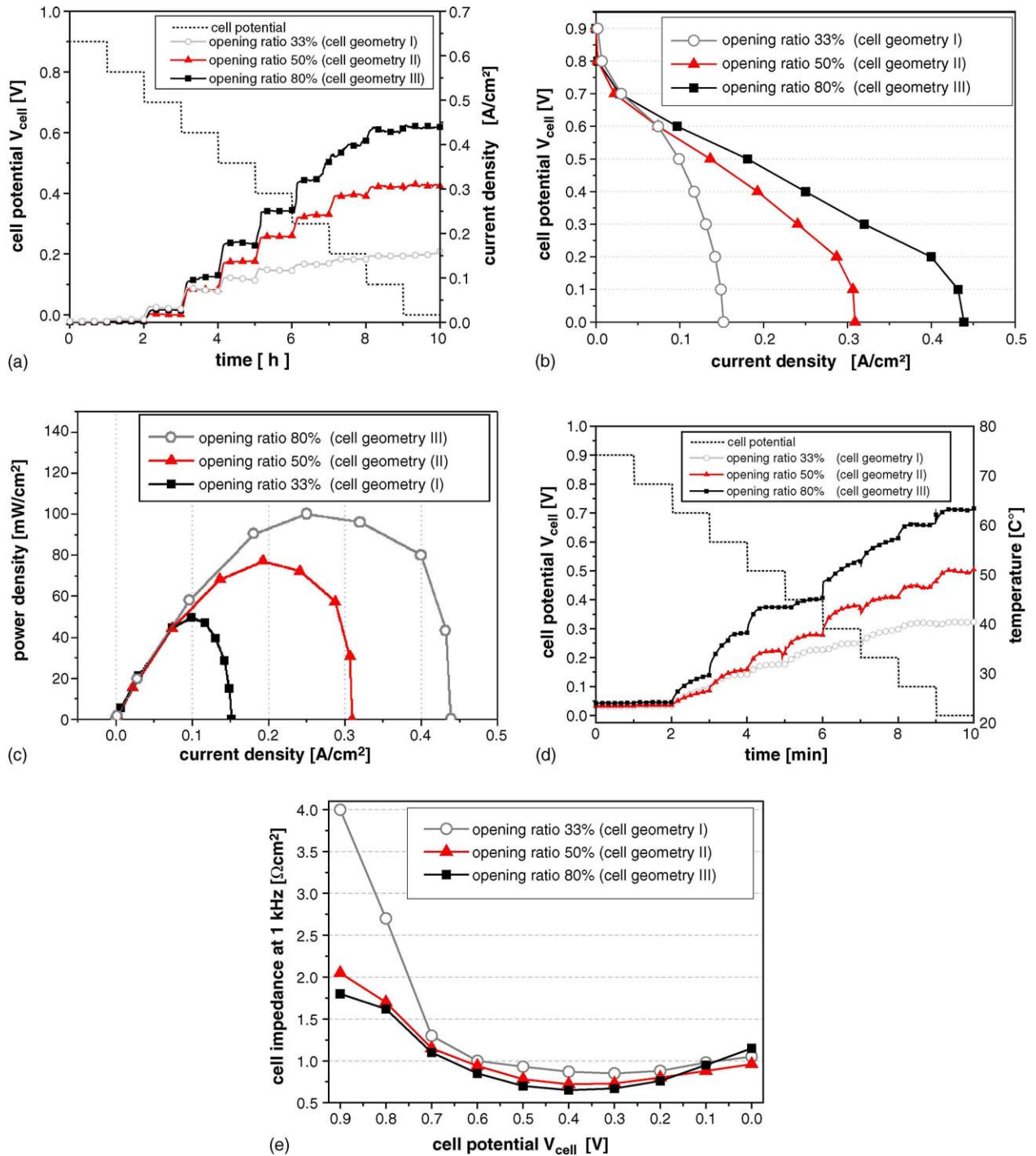
Fig. 4. (a) Development of current density for cell samples with an opening ratio of 33%, 50% and 80% by applying a constant potential for a period of 1 h (potential step method). (b) Polarisation curves extracted from the potential step measurements of the cell samples with opening ratios of 33%, 50% and 80%. (c) Power characterisitcs extracted from the potential step measurements of the cell samples with opening ratios of 33%, 50% and 80%. (d) Development of cell temperature for cell samples with an opening ratio of 33%, 50% and 80% by applying a constant potential for a period of 1 h (potential step method). (e) Behaviour of cell impedance (at 1 kHz) for the three opening ratios during the long-term potential step measurements.

The behaviour of the impedances for all cells in the range of 0.5–0 V is similar. A minimum of cell impedance exists between 0.4 and 0.3 V. Following the minimum, a slight increase of the impedance is seen. For the cell with the largest opening the minimum and the subsequent increase is most distinct, as this

type of cell generates the highest current densities, the highest amount of water is produced. The increased water production in turn results in a well-humidified membrane and a minimum of the cell impedance. The subsequent distinct increase in cell impedance is a result of the increased temperature (Fig. 4c).

At high temperatures, the evaporation of water is significantly faster which, leads to a drying out of the cell and increased cell impedances.

The increased impedances for low cell potentials (<0.3 V) represent major Ohmic losses. Other losses in this operation range are caused by mass transport limitations (see above).

5. Water balance measurements

According to the electrochemical reaction, water is produced in the catalyst layer of the cathode. Water is exchanged through the membrane between cathodic and anodic side by diffusion and electro-osmotic drag [12]. As a result water is removed from the cell by an anodic and cathodic water flux. At the anodic side, water vapour and the droplets of condensed water are extracted by the convective gas flow. From the open cathode, the water can be removed by diffusion. The fluxes removing water from the anodic and cathodic side strongly depend on the cell conditions.

An experimental water balance can be set-up by collecting the water, which is removed from the anode and cathode over a period of time. As it is not feasible to collect the water from the open cathode, only the water leaving the anodic outlet with the hydrogen flow was determined by condensation. The entire water production in this period of time is determined according to Faraday's law [8] by the total cell current. Hence, the water removed from the cathode can be calculated by subtraction.

The condensation of water at the anodic outlet was realised by passing the hydrogen flow through a glass bulb, which was submerged in a cooling liquid. The liquid was cooled down to $-5\,^\circ$C by the use of a cryostat. The relative humidity at the outlet of the bulb was measured by a sensor and found to be less than 10% at a gas temperature of 5 $^\circ$C. According to the function of the saturation pressure [11] almost the entire water in the hydrogen flow was condensed in the glass bulb.

At the end of the operation period the anode flow-field has been rinsed with a high flow of hydrogen in order to remove the water droplets remaining in the anode compartment. The accumulated water in the bulb was determined by weighing.

The collection of water at the anode was carried out for cell samples with opening ratios of 33%, 50% and 80%. These cell samples were operated at different operation points. The cells with an opening ratio of 50% and 80% were operated at a constant load of 1.0 A (0.1 A cm^{-2}), 2.0 A (0.2 A cm^{-2}) and 2.5 A (0.25 A cm^{-2}). The cell with the 33% opening ratio was operated at a constant load of 0.5 A (0.05 A cm^{-2}), 1.0 A (0.1 A cm^{-2}) and 1.5 A (0.15 A cm^{-2}).

In each experiment, the cells were operated for a period of 8 h. Subsequently the amount of condensed water of the anode gas flow was determined. The total amount of water produced according to Faraday's law in a period of 8 h at a current of 1.0, 2.0 and 2.5 A accounts for 2.7, 5.4 and 6.7 g, respectively. At cell currents of 0.5 and 1.5 A the total amount of water produced in 8 h accounts for 1.35 and 4.05 g, respectively.

Results of the water balance measurements for cells operated in a horizontal position (open cathode upside) are shown in Fig. 5a and b. In Fig. 5a, the calculated total water production (hatched bars) and the amount of water condensed at the anode
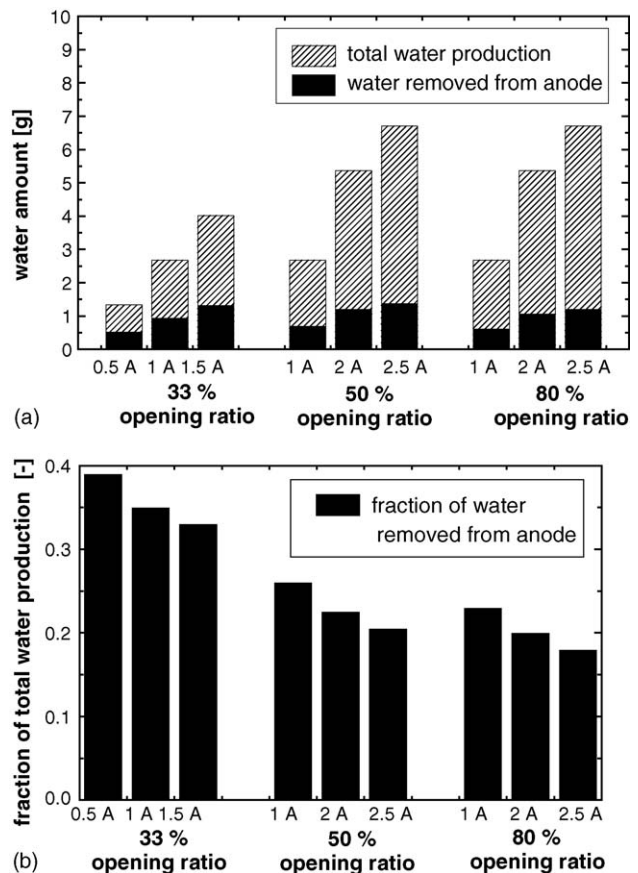

Fig. 5. (a) Water balance for test cells with opening ratios 33%, 50% and 80% under constant constant load of 1, 2 and 2.5 A for horizontal cell position. (b) Fraction of the total water production removed from the anode. The calculations are based on the values shown in Fig. 5a.

outlet (black bars) are depicted. The amount of water removed over the cathode is marked by the difference of both shown bars.

Based on the data of Fig. 5a, the fraction of water removed from the anode is obtained and depicted Fig. 5b. This fraction is calculated as the ratio between the amount of water removed from the anode and the total water production.

As can be seen from Fig. 5b, the fraction of water removed from the anode for the largest opening ratio (80%) is about 20%. For the cells with the two smaller opening ratios a fraction of about 25–35% of the total water production is removed via the anode. For all three-cell geometries, the fraction of the water removed from the anode decreases slightly with increasing current densities. Based on these results one can conclude that the majority of the water is removed from the open cathode for all opening ratios and operation points.

The results shown in Fig. 5a and b were obtained for cells operated in a horizontal position with the open cathode side faced up. As the orientation of the cells may have an effect on the water balance, the cells were additionally operated in a vertical position. In a vertical position condensed water droplets have the ability to drip off the cell. The cells operated in vertical position had the same values and fractions as the cells operated in the horizontal position (see Fig. 5a and b) [13].

Based on these similarities, it is concluded that the majority of the water on the cathode is removed by diffusion, and that only a minor fraction of the water is removed by condensed droplets that drip off the cell.

6. Influence of hydrophobic and hydrophilic diffusion layers

The wetting properties of water on a surface differ depending on the properties of the surface. Wetting properties are quantified by the concept of contact angle. The contact angle is defined as the angle between the surface and the tangent to the shape of the droplet at its edge where the liquid contacts the surface [14]. In the case of water, hydrophobic surfaces are characterised by wetting angles with $\theta > 90°$, while for hydrophilic surfaces the wetting angles are $\theta < 90°$.

The GDL plays a key role in providing good access of reactants towards the electroactive sites and effective removal of product water from the electrode. Previous studies have demonstrated the importance of wetting properties and morphology of GDLs [15–19]. These studies show that altering the composition of the GDL can lead to substantial improvements in cell performance. The improvements reported relate to differences in the fabrication process of coated GDL like the PTFE content, the morphology of the carbon black and the effect of sintering, as well as physical differences like the pore-size distribution and the thickness of the GDL. An overview of previous work is given by Jordan et al. [18].

Nevertheless, the previous studies have in common that they characterised the GDLs in a conventional PEMFC design with a closed cathodic compartment that was supplied by a convective flow of air or oxygen. In contrast, this work focuses on air-breathing PEMFC and how its performance is influenced by GDLs having different wetting properties. The performance of air-breathing PEMFCs with hydrophobic and hydrophilic GDLs are characterised and compared to the performance of air-breathing PEMFCs with normal GDL.

The GDLs with hydrophobic and hydrophilic properties were prepared using the following described methods. The preparations were made by coating of Toray® carbon paper TGP-H-120 (thickness 350 μm). The hydrophobic properties were achieved by dispensing a suspension of PTFE (10%) and nano-sized carbon particle powder (Vulcan XC-72R carbon black) on the carbon paper [13]. The GDL was then sintered at 390 °C for 15 min.

Gas diffusion layers with hydrophilic properties were prepared by immersing carbon paper in a solution of tungsten–ormosilane [13]. A reproducible coating thickness was achieved by repeated plunging the GDL in the solution using a robot. Subsequently, the GDLs were tempered at 450 °C for 30 min.

The behaviour of a water droplet on the hydrophobic and hydrophilic GDL can be seen in Fig. 6a and b. The droplet on the hydrophobic GDL (Fig. 6a) is rejected by the surface, whereas, the droplet on the hydrophilic GDL (Fig. 6b) is absorbed completely.

SEM images of an untreated and a hydrophobic GDL are shown in Fig. 7a and b. The SEM picture of the hydrophobic GDL reveals that the carbon fibres and some voids are covered
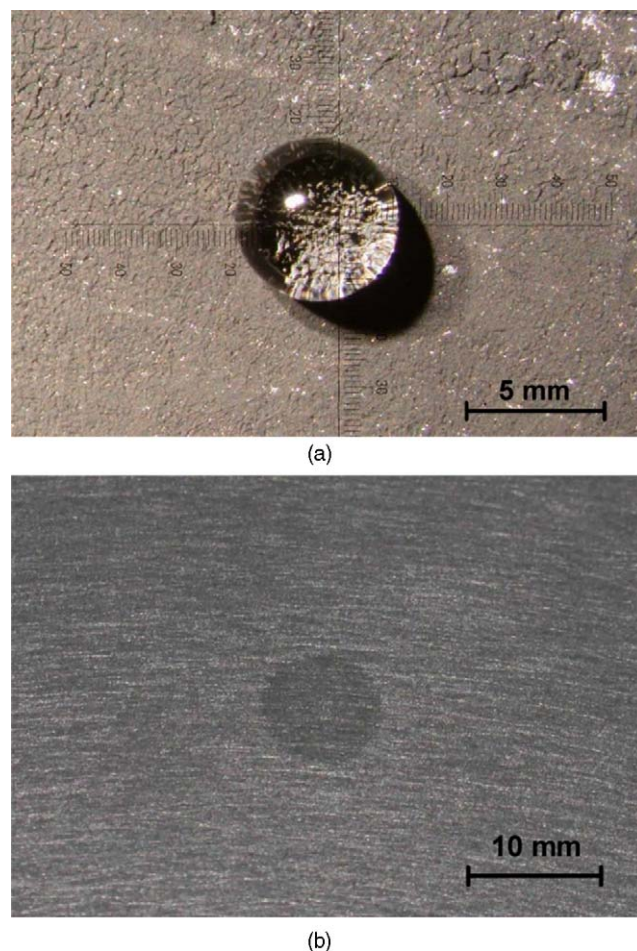

Fig. 6. (a) Behaviour of a water droplet on a hydrophobic GDL. A water droplet dispensed on the GDL remains on the surface and does not get absorbed. (b) Behaviour of a water droplet on a hydrophilic GDL. On the hydrophilic GDL, the water droplet is immediately sucked in the carbon paper and dissipates over a surface several millimeters in diameter.

by melted PTFE polymer. Hence, it is concluded that the porosity of the treated GDLs has decreased in comparison to the untreated GDLs.

Due to the chemical treating of the GDL, a change in the contact resistance can be expected. The contact resistance between the metallic layer of the PCB and the GDLs were analysed to quantify this change. In order to passivate the copper layers against corroding, the PCBs were coated. In long-term characterisations a coating with Cr was found to be most suitable for passivation in the fuel cell environment [6,7]. For the measurement of the electrical contact resistance, a GDL was positioned between two coated PCBs (area 2 cm × 2 cm). This sandwich was clamped in a pressure apparatus in which the applied pressure could be measured using a piezoelectric sensor. With this procedure, the resistance of the GDLs as a function of compression pressure was measured for a hydrophobic, hydrophilic and untreated GDL. The results obtained for Cr-coated PCB plates are depicted in Fig. 8.

The resistance, as a function of compression pressure, shows a similar development for all characterised GDLs. At small pressures, a steep decline of resistance with pressure is observed,
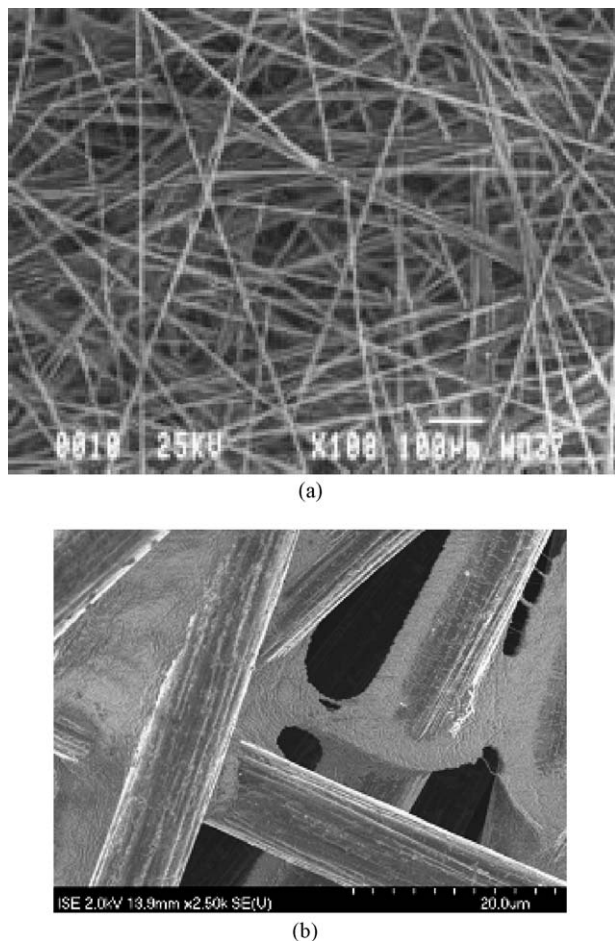
(a)

(b)

Fig. 7. (a) SEM images of the untreated GDL. (b) SEM image of the hydrophobic coated GDL.

whereas, for pressures larger than 0.2 MPa, only a slight decrease of resistance with pressure is seen. At a pressure of 0.8 MPa, the surface specific resistance for the Cr-coating accounts for 160 mΩ cm^2 for the untreated GDL, 180 mΩ cm^2 for the hydrophilic GDL and 230 mΩ cm^2 for the hydrophobic GDL.

Based on the specific electrical conductivity of the carbon paper TGP-H-120 of $\sigma = 1250\,\Omega^{-1}\,m^{-1}$ [20], the specific sur-
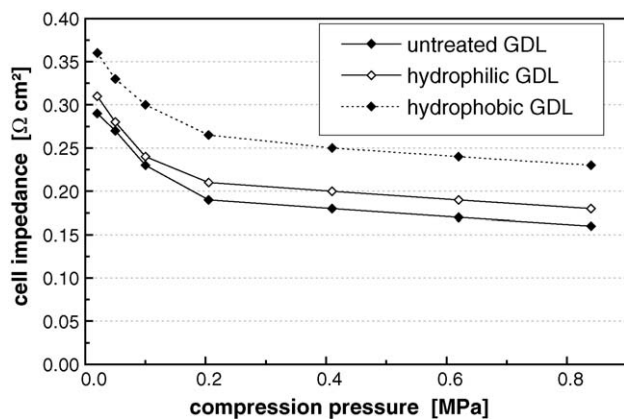

Fig. 8. Dependence of the specific contact resistance on applied pressure for an untreated, hydrophobic and hydrophilic GDL located between two PCB plates, which are coated with Cr.

face resistance of the carbon paper can be calculated to be 2.8 mΩ. Thus, it can be concluded, the measured specific surface resistances are mostly due to contact resistances between the GDL and the coated PCB plate.

The higher contact resistances for the hydrophobic and hydrophilic GDLs can be explained by the treatment with the non-conducting coatings, which lead to an increased contact resistance.

In order to see the influence of the changed surface properties of the GDLs on the performance of the air-breathing PEMFC the operation behaviour was measured. The treated GDLs were used only on the cathodic side, while untreated GDLs were applied on the anode throughout all measurements. The characterisations were carried out with the potential step method under floating temperature conditions. In this manner, the coated GDLs were characterised for the three different opening ratios (cell geometries I–III). In Fig. 9a–c, the results of the measurements are depicted together with the results from the untreated GDLs, which have been already presented in Fig. 4a.

For all opening ratios and throughout the whole operation range, the highest current densities are seen for the untreated GDL. Moreover, the current densities for the hydrophobic GDL are always higher than for the hydrophilic GDL.

Current densities achieved at short-circuit conditions for the cell with the largest opening ratio (80%) were 0.4 A cm^{-2} for the untreated GDL, 0.33 A cm^{-2} for the hydrophobic GDL and 0.28 A cm^{-2} for the hydrophilic GDL. In comparison, for the cell with the smallest opening ratio (33%) the obtained current densities at short-circuit conditions were only 0.16 A cm^{-2} for the untreated GDL, 0.1 A cm^{-2} for the hydrophobic GDL and 0.08 A cm^{-2} for the hydrophilic GDL.

Additionally, the cell impedances at 1 kHz for the three different GDLs and the opening variations were measured (see Fig. 10). For all test samples, decreasing cell impedances are seen from cell potentials of 0.9 V to about 0.5 V. As pointed out above in the case of the untreated GDL (Fig. 4d) this behaviour is consistent with a self-humidifying of the membrane. Moreover, the significantly high impedance values for the lowest opening ratio are explained by the constricted exchange with humid ambient air.

For cell potentials of 0.5–0 V the differences in the cell impedances depending on the surface properties of the GDLs are significant. The impedance for the cell with the hydrophobic GDL slightly decreases, whereas, the impedance for the untreated and hydrophilic GDLs passes through a minimum at 400 mV and then increases. For the hydrophilic GDL the cell impedance increases very steeply; the cell impedance for the untreated GDL, in contrast, increases moderately.

The comparatively lower current densities of the cells with the treated GDLs can be explained by the higher contact resistances (see Fig. 8) and by the reduced porosity due to the applied coating substances.

Although the hydrophobic GDL is characterised by a larger contact resistance than the hydrophilic GDL, higher current densities were achieved with the hydrophobic GDL than with the hydrophilic GDL. This result indicates that the variations in performance are not caused by differences in contact resistances.
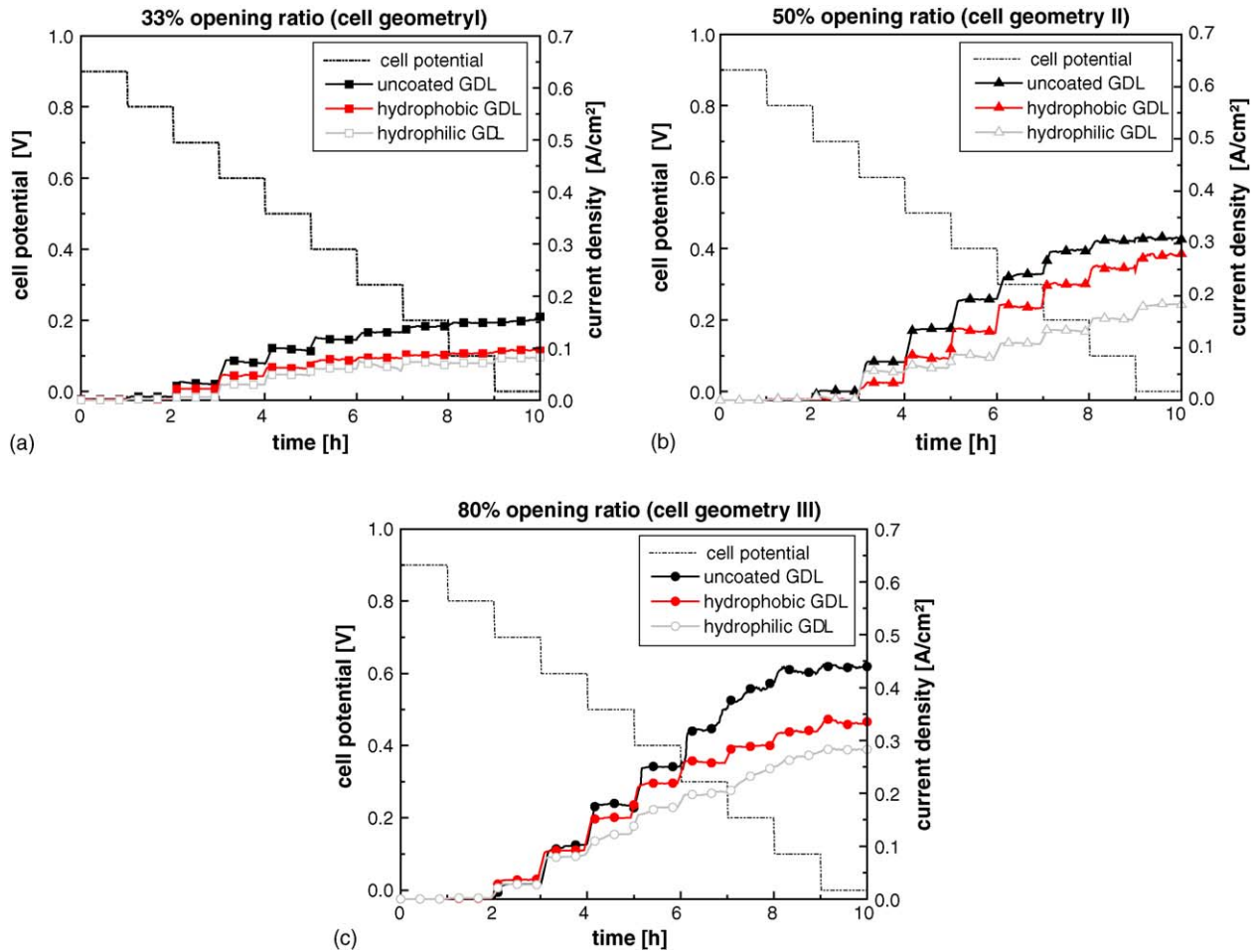
Fig. 9. (a) 33% opening ratio (cell geometry I); (b) 50% opening ratio (cell geometry II); (c) 80% opening ratio (cell geometry III). (a–c) Development of the cell current measured for the untreated, hydrophobic and hydrophilic GDLs for the opening ratios of 33%, 50% and 80% according to the potential step method.

Since, the hydrophilic GDL is able to absorb the produced water into its pores, its porosity is significantly reduced and consequently the diffusion of oxygen to the cathode is impeded.

This behaviour is reflected in the characteristic of the cell impedance at 1 kHz. As the cell potential decreases, more heat is produced inside the cell resulting in a rise in temperature. Due to the absorption of the produced water in the hydrophilic GDL, the water is distributed over a large surface and can evaporate more efficiently. Thus, the cell dries out faster at increasing temperatures, and consequently the cell impedance increases.

For the hydrophobic GDL the reverse situation applies. Due to the hydrophobic surface properties the water produced in the catalyst layer cannot be absorbed in the GDL and a film of water emerges on the surface of the MEA. This film of water keeps the MEA well humidified but hinders the oxygen supply to the catalyst layer and consequently leads to a reduced current generation. Moreover, as the water film has a smaller surface area, it cannot evaporate as efficiently despite the increasing temperatures. As a result the MEA stays well humidified, and even a slight decrease in cell impedance is observed with decreasing cell potentials.

The above argumentation is supported by measurements of the cell's water balance. Analogously to Section 5, the amount

of water removed from the anode has been determined for a period of 8 h. According to that procedure the three different GDLs were characterised in a cell with the largest opening ratio (80%) using current densities of 0.1 A cm^{-2} (1 A cell current), 0.2 A cm^{-2} (2 A cell current) and 0.25 A cm^{-2} (2.5 A cell current), respectively. Fig. 11 shows the amount of water removed from the anode for each type of GDL at the three current densities and the respective total water production. At the three current densities the same effect is seen. The highest amount of water is removed from the cathode using the hydrophobic GDL, and the lowest amount of water is removed using the hydrophilic GDL. Since, the hydrophilic GDL has the ability to absorb condensed water, only a low fraction of water can permeate through the membrane. Furthermore, as the hydrophobic GDL rejects the liquid water produced in the catalyst layer, a larger fraction of water diffuses from the cathodic to the anodic side. Thus, the above argumentation concerning the behaviour of the cell impedance is supported by the measurement of the water balance.

It can be concluded that the wetting properties itself have an intense influence on the performance of an air-breathing PEMFC. Both, hydrophobic and hydrophilic GDLs cause mass transport problems in air-breathing PEMFC. The hydrophilic
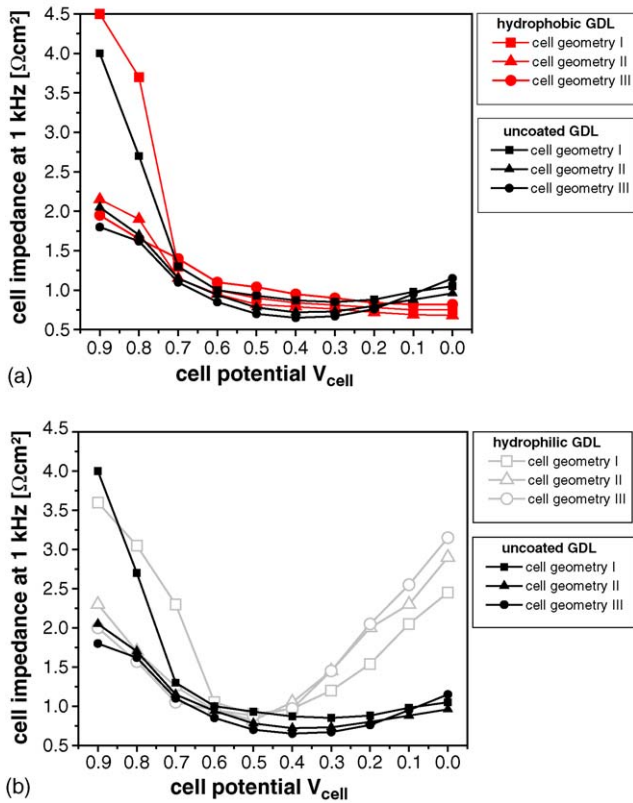
Fig. 10. (a) Cell impedances for the uncoated and hydrophobic GDLs for cell with opening ratios of 80%, 50% and 33% (cell geometries I–III). (b) Cell impedances for the uncoated and hydrophilic GDLs for cell with opening ratios of 80%, 50% and 33% (cell geometries I–III).

GDL absorbs liquid water and thus reduces the porosity. With a hydrophobic GDL, mass transport problems occur, since a film of liquid water can cover the catalyst layer. Additionally, higher contact resistances and reduced porosities caused by the coating, result in lower cell performance using hydrophobic and hydrophilic GDLs.

7. Conclusion

Due to their passive operation, air-breathing fuel cells show promising perspectives as miniaturised power sources in electronic devices. Air-breathing PEMFCs can be realised in a rather flat design using PCB technology. With the reliable and flexible mass production process of PCB technology, miniaturised PEMFCs can be manufactured at low costs and in a variety of cell designs. A series connection of planar arranged cells can be easily realised using multilayer PCB technology. Planar air-breathing PEMFCs are ideal for an integration into the housing of a device. Thus, volume needed for the power source can be optimised.

The passive supply of oxygen makes the use of power consuming fans and pumps obsolete. However, due to the openings to the exterior, the design of the cathode is crucial to optimise the performance of the cell. In this paper, the operation behaviour of air-breathing PEMFCs with different opening sizes and different wetting properties of gas diffusion layers (GDL) were characterised.

In the first part, cell samples with opening ratios of 33%, 50% and 80% and a standard GDL (untreated Toray® carbon paper TGP-H-120, thickness of 350 μm) were characterised by measurements of the current density, the temperature, the cell impedance and the water balance. Distinct differences in performance between the opening ratios are seen. Larger opening ratios result in higher current densities and cell temperatures at corresponding cell potentials. The current density at short circuit conditions of the cell with the highest opening ratio (80%) is $0.44 \, \mathrm{A \, cm^{-2}}$. This is more than three times larger than the one in the case of the smallest opening ratio (33%). The cell temperature at short circuit conditions for the cell with the 80% opening ratio was 63 °C.

The development of the cell impedance as a function of cell potential has a rather similar shape for all three opening ratios. Starting from open circuit condition, the cell impedances decreases with declining cell impedances and passes through a minimum around cell potentials of 0.4–0.3 V. This behaviour reflects that with increasing water production, the humidification of the membrane augments. A subsequent slight increase in cell impedance is caused by a drying out of the membrane due to the increased cell temperature. Water balance measurements showed that most of the water produced is removed at the anode, while a small amount is removed at the cathode by gas diffusion.

In the second part, the influence of GDLs with hydrophilic and hydrophobic properties (chemically treated Toray® TGP-H-120) on the cell performance were characterised and compared to the results of cells with untreated GDLs for opening ratios of 33%, 50% and 80%. The cells with the untreated GDLs showed for all opening ratios, a higher current density than the cells with hydrophobic and hydrophilic GDLs. Cells with the hydrophobic GDL achieved a slightly better performance compared to the cell with the hydrophilic GDL.
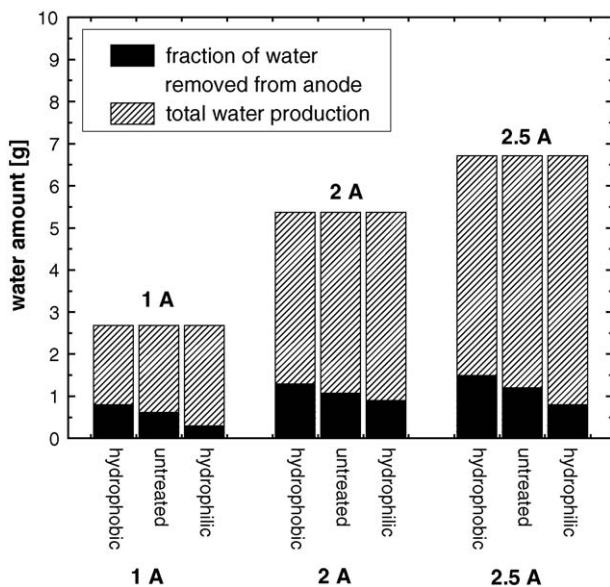

Fig. 11. Water drag out for the untreated, hydrophobic and hydrophilic GDL at different current densities measured with the cell with the 80% opening ratio.

The poorer performance of cells with hydrophobic and hydrophilic GDLs can partially be explained by their higher contact resistances and decreased porosities compared to untreated GDL material.

A more intense influence was found to result from the wetting properties itself. The hydrophilic GDL has the ability to absorb the condensed water in the GDL. This results in a reduced porosity of the GDL and a hindered supply of oxygen. Moreover, with the hydrophilic GDL the membrane has the tendency to dry out, as the water produced in the MEA is sucked in the GDL. This behaviour is reflected in rapidly increasing cell impedances at low cell potentials for the cells with hydrophilic GDLs.

With the hydrophobic GDL, condensed water cannot be absorbed in the GDL. Consequently, a film of water evolves which keeps the membrane well humidified, but also hinders the supply of oxygen. This interpretation is supported by the significant low cell impedances for the cells with hydrophilic GDLs.

The best performance for air-breathing operation was achieved using an untreated Toray® GDL (TGP-H-120). Due to the slight hydrophobic properties of the untreated GDL, the membrane can be kept well humidified, but the oxygen supply does not get significantly blocked by a film of water. Moreover, the untreated GDL is characterised by a higher porosity and lower contact resistances compared to the treated GDLs. The combination of these properties result in a superior performance of the untreated Toray® GDL.

The maximum power density of all samples ($100 \, \text{mW cm}^{-2}$ at a cell potential of 0.4 V) was achieved with the opening ratio of 80% using an untreated GDL. The cell temperature measured at this the maximum power point was about $43 \, °\text{C}$ which corresponds to a temperature slightly higher than the human body temperature.

Concerning the water management it was shown that only a minor amount of the produced water ($<25 \, \%$ for an opening ratio of 80%) is removed over the open cathode, mostly in the form of vapour. This fact is important to underline as it confirms that a wetting or flooding of the exterior of an air-breathing PEMFC is very unlike to happen. Hence, concerning the temperature and the water emitted to the exterior, it can be concluded that the operation of an air-breathing PEMFC is very well suited to be operated in an indoor environment.

Based on the presented characterisations, important conclusions on design rules of air-breathing hydrogen fuelled PEMFCs can be drawn. First, it is crucial to design the cathode opening as large as possible, whereby the opening ratio of the cathode can be increased as long as an appropriate compression pressure of the cell assembly and therewith a low contact resistance can be assured.

Second, GDLs with hydrophilic or an intense hydrophobic properties do not improve the performance of an air-breathing PEMFC, whereas, the usage of a slight hydrophobic untreated GDL is more beneficial.

References

[1] C.K. Dyer, J. Power Sources 106 (2002) 31–34.
[2] A. Heinzel, et al., J. Power Sources 105 (2002) 250–255.
[3] A. Schmitz, S. Wagner, R. Hahn, M. Tranitz, C. Hebling, Miniaturized planar fuel cell with self-breathing cathode side, in: Proceedings Fuel Cell Seminar 2002, Palm Springs, USA, 2002.
[4] R. O'Hayre, D. Braithwaite, W. Hermann, S.-J. Lee, T. Fabian, S.-W. Cha, Y. Saito, F.B. Prinz, J. Power Sources 124 (2003) 459–472.
[5] A. Schmitz, R. Hahn, C. Hebling, B. Burger, German patent application number, DE 102 17 034.7, Brennstoffzellensystem in Leiterplattenbauweise, 11 April, 2002.
[6] A. Schmitz, S. Wagner, et al. Stability of Planar PEMFC in Printed Circuit Board Technology, Poster presentation, Ulm 8th Electrochemical Talks, Ulm, Germany, June 19–20, 2002.
[7] A. Schmitz, S. Wagner, R. Hahn, H. Uzun, C. Hebling, J. Power Sources 118 (2003) 162–171.
[8] W. Vielstich, A. Lamm, H.A. Gasteiger, Handbook of Fuel Cells—Fundamentals Technology and Applications, vol. 1, Wiley, 2003.
[9] C.H. Hamann, W. Vielstich, Electrochemistry, Wiley-VCH, Weinheim, 1998.
[10] R.B. Bird, W.E. Stewart, E.N. Lightfoot, Transport Phenomena, 2nd ed., Wiley, New York, 2001.
[11] H.D. Baehr, Thermodynamik, Springer-Verlag, Berlin, 2004.
[12] T.A. Zawodzinski, J. Electrochem. Soc. 140 (4) (1993).
[13] M. Tranitz, Aufbau und Charakterisierung von Brennstoffzellen in Leiterplattenbauweise, Diploma Thesis, Freiburg, 2003.
[14] D. Myers, Surfaces, Interfaces and Colloids, Wiley-VCH, New York, 1999.
[15] M.S. Wilson, J.A. Valerio, S. Gottesfeld, Electrochim. Acta 40 (1995) 355–363.
[16] V.A. Paganin, E.A. Ticianelli, E.R. Gonzalez, J. Appl. Electrochem. 26 (1996) 297–304.
[17] L. Giorgi, E. Antolini, A. Passalacqua, Electrochim. Acta 43 (1998) 3675–3680.
[18] L.R. Jordan, A.K. Shukla, T. Behrsing, N.R. Avery, B.C. Muddle, M. Forsyth, J. Appl. Electrochem. 31 (2001) 449–454.
[19] D. Bevers, M. Wöhr, K. Yasuda, K. Oguro, J. Appl. Electrochem. 27 (1997) 1254–1264.
[20] M.F. Mathias, J. Roth, J. Fleming, W. Lehnert, Diffuison media materials and characterisation, in: W. Vielstich, A. Lamm, H.A. Gasteiger (Eds.), Handbook of Fuel Cells—Fundamentals, Technology and Applications, vol. 1, Wiley, 2003.